



ELSEVIER

Physics of the Earth and Planetary Interiors 102 (1997) 201–212

PHYSICS  
OF THE EARTH  
AND PLANETARY  
INTERIORS

# Transitions in thermal convection with strongly variable viscosity

James Todd Ratcliff <sup>a,\*</sup>, Paul J. Tackley <sup>a,1</sup>, Gerald Schubert <sup>a,b,2</sup>,  
Abdelfattah Zebib <sup>c,3</sup>

<sup>a</sup> Department of Earth and Space Sciences, University of California, Los Angeles, CA 90095-1567, USA

<sup>b</sup> Institute of Geophysics and Planetary Physics, University of California, Los Angeles, CA, USA

<sup>c</sup> Department of Mechanical and Aerospace Engineering, Rutgers University, Piscataway, NJ 08855-0909, USA

Received 20 September 1996; accepted 28 February 1997

## Abstract

One of the most important material properties influencing the style of convection in the mantles of terrestrial planets is the extreme temperature-dependence of viscosity. Three-dimensional numerical convection calculations in a wide ( $8 \times 8 \times 1$ ) cartesian box and in a spherical shell (ratio of inner to outer radius of 0.55, characteristic of terrestrial planets) both display two fundamental transitions as the viscosity contrast is progressively increased from unity to a factor of  $10^5$ . These transitions not only mark changes in the style of deformation in the upper boundary layer from mobile-lid to sluggish-lid to stagnant-lid but also have dramatic effects on the style, planform, and horizontal length scales of convection in the entire domain. Vertical variations of viscosity are the most important for determining the horizontal length scales of the convective patterns while lateral viscosity variations play a role in shaping the relative structures of the upwelling and downwelling flows. Convection in Venus appears to be represented most closely by the sluggish-lid regime of convection, whereas the Earth, with plate tectonics, more closely resembles the mobile-lid style of convection. Forcing plate-like characteristics onto the convective flows in the form of imposed weak zones and prescribed surface velocities results in flow patterns dominated entirely by the form used to enforce the plate-like behavior and tells us little about why the mantle exhibits long-wavelength heterogeneity. © 1997 Elsevier Science B.V.

## 1. Introduction

The relationship between the convective motions of the interiors of terrestrial planets and the surface tectonics of the planets (or lack thereof) is a funda-

mental question in planetary geophysics. That the rheology of mantle material is strongly dependent on temperature has been understood for several decades (Weertman, 1970; Weertman and Weertman, 1975). This temperature dependence is likely to exert a pronounced influence on the style of thermal convection in terrestrial mantles and hence greatly affect the nature of the surface expression of such convection. Laboratory studies of thermal convection with temperature-dependent viscosity have been undertaken for rigid boundary conditions (Booker, 1976; Richter, 1978; Richter et al., 1983; Stengel et al., 1982;

\* Corresponding author. Tel.: +1-310-825-3118; fax: +1-310-825-2779; e-mail: todd@artemis.ess.ucla.edu.

<sup>1</sup> E-mail address: tackley@ess.ucla.edu.

<sup>2</sup> E-mail address: schubert@ucla.edu.

<sup>3</sup> E-mail address: zebib@jove.rutgers.edu.

White, 1988) and for stress-free upper boundaries (Weinstein and Christensen, 1991; Giannandrea and Christensen, 1993). However, the limited range of material properties and the rigid boundary conditions in these investigations limit their applicability to realistic planetary mantles.

Numerical models of three-dimensional convection with temperature-dependent viscosity which possess more realistic free-slip conditions at both boundaries have, until recently, been restricted to steady-state solutions in small aspect ratio boxes (Christensen and Harder, 1991; Ogawa et al., 1991). These calculations remain problematic for application to terrestrial mantles, however, since model aspect ratio can greatly affect convective planform independently of any rheological behavior. Numerical investigations of three-dimensional, time-dependent convection with temperature-dependent viscosity in large aspect ratio, cartesian geometry have lately been undertaken (Balachandar et al., 1995a,b; Tackley, 1993, 1996a) but have been limited to relatively small viscosity contrasts (of order 1000 or less). Studies of convection with temperature-dependent viscosity which employ a more realistic spherical geometry are even fewer in number. Investigations have been performed for two-dimensional axisymmetric convection in a spherical shell (Hsui, 1978; Machetel and Rabinowicz, 1985; Zebib, 1993). For fully three-dimensional convection in a spherical shell, steady (Ratcliff et al., 1996b) and weakly time-dependent calculations (Ratcliff et al., 1995, 1996a) have begun to appear only very recently.

Here, a set of time-dependent, three-dimensional calculations in both spherical geometry (spherical shell with ratio of inner to outer radius,  $\eta = 0.55$ ) and large aspect ratio cartesian geometry ( $8 \times 8 \times 1$  box) are presented which illustrate the dramatic transitions in convective style that occur as the viscosity contrast (ratio of surface viscosity to basal viscosity) across a convecting layer is increased by up to a factor of  $10^5$  ( $10^4$  in the spherical shell). The relative importance of vertical versus horizontal viscosity variations on these plan-form transitions is also explored. In addition, other conditions that can drastically alter the style of convection in planetary mantles are examined; these conditions include imposed weak zones (analogous to lithospheric faults) and prescribed plate-like boundary conditions.

## 2. Convection models

While the mantle of the Earth is predominantly heated from within by the decay of radioactive elements (Schubert, 1979), it is difficult in internally heated convection to establish a consistent temperature scale for determining the thermally activated viscosity variation. Since the maximum temperature in an internally-heated system is not known a priori, the maximum viscosity contrast remains unknown as well. Because it is the effects of variable viscosity on mantle convection which are of interest here, it is more convenient to select a system in which the temperature variations are known in advance. For this reason we consider thermal convection in a basally-heated fluid layer. The study by Ratcliff et al. (1996a) in which both basal heating and mixed-mode heating (internal and basal heating) are examined indicates that such a choice will not have dramatic effects on the large-scale phenomena discussed in this paper.

Boundary conditions on the upper and lower surfaces of the fluid layer are free-slip, impermeable and isothermal. Calculations are carried out in three dimensions in both a cartesian box and a spherical shell. Side boundaries in the cartesian box are periodic. An infinite Prandtl number, as is appropriate for the mantles of terrestrial planets (Schubert, 1979; Busse, 1989), is assumed and the Boussinesq approximation (relaxed to permit a temperature-dependent and therefore spatially variable viscosity) is employed to simplify the equations for conservation of mass, momentum, and energy. Convective vigor is characterized by the Rayleigh number

$$\text{Ra}_{1/2} = \frac{\rho g \alpha \Delta T D^3}{\kappa \mu_{1/2}}, \quad (1)$$

where  $\rho$  is the density,  $g$  is the acceleration due to gravity,  $\alpha$  is the coefficient of thermal expansion,  $\Delta T$  is the temperature difference across the layer,  $D$  is the layer thickness,  $\kappa$  is the thermal diffusivity, and  $\mu_{1/2}$  is the reference dynamic viscosity. The subscript 1/2 indicates that the Rayleigh number is defined for a reference viscosity  $\mu_{1/2}$  taken at the average of the upper and lower boundary temperatures. The system is made dimensionless via scaling of length, temperature, and time by  $D$ ,  $\Delta T$ , and

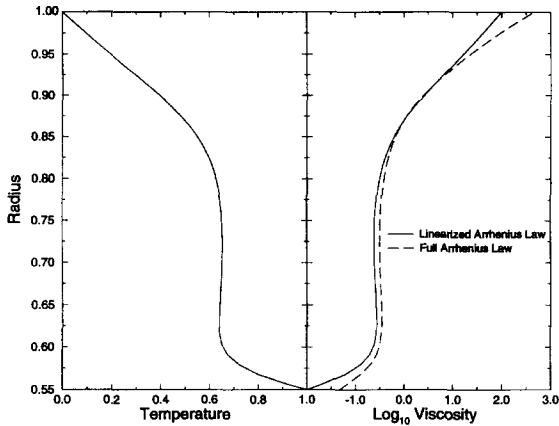


Fig. 1. The differences between the full Arrhenius rheology and the linearized Arrhenius rheology. The temperature profile is from a spherical-shell convection calculation with  $\Delta\mu = 10^4$ .

$D^2/\kappa$  (the thermal diffusion time), respectively. Velocities, in turn, are scaled by  $\kappa/D$ , and the pressure scaling assumes pressure gradients are comparable to viscous stresses (scaling pressure by  $\mu_{1/2}\kappa/D^2$ ).

For calculations in spherical geometry, the dimensionless viscosity is assumed to vary with nondimensional temperature  $T$  (ranging from  $T=0$  at the upper boundary to  $T=1$  at the lower boundary) according to a linearized Arrhenius law of the form

$$\mu(T) = \exp[-E(T - 0.5)], \quad (2)$$

where the activation parameter  $E = \ln(\Delta\mu)$  and the viscosity contrast  $\Delta\mu = \mu(T=0)/\mu(T=1)$ . Calculations in cartesian geometry utilize the full Arrhenius law

$$\mu(T) = \exp\left[E\left(\frac{1}{T+1} - \frac{1}{1.5}\right)\right], \quad (3)$$

where  $E = 2 \ln(\Delta\mu)$ . The effects that these different rheological laws impose on the viscosity structure is illustrated in Fig. 1, using the horizontally-averaged temperature structure from a spherical-shell convection calculation with  $\Delta\mu = 10^4$ . The effect on the viscosity due to linearization of the Arrhenius law is to lessen the magnitude of the viscosity contrast across the cold thermal boundary layer, i.e., more of the total  $\Delta\mu$  is taken up by the hot thermal boundary layer compared to the full Arrhenius law. The average viscosity structures differ only slightly and should

lead to qualitatively similar results between the cartesian and spherical-shell calculations.

The equations for conservation of mass, momentum, and energy are solved numerically via two computer models. In spherical geometry, the three-dimensional finite-volume model used in Ratcliff et al. (1995, 1996a,b) is employed. The spherical shell is subdivided into 40 radial, 50 latitudinal and 100 longitudinal control volumes with uniform grid spacing. Adequate horizontal resolution for the spherical calculations is confirmed by noting that the spherical harmonic power spectra of temperature variance for all calculations show several orders of magnitude decrease in power at the highest spherical harmonic degrees. This indicates that near-grid-scale (i.e., under-resolved) phenomena are not present in the calculations. In addition, vertical resolution is deemed adequate since five to eight grid points occur within the smallest boundary layers. A second order Crank–Nicolson scheme is used for implicit timestepping and a relaxation scheme based on the SIMPLER algorithm of Patankar (1980) is used to resolve the nonlinear coupling between the conservation equations during each timestep. See Ratcliff et al. (1996a,b) for further discussion of the numerical model used for the spherical-shell calculations.

For the cartesian calculations, the three-dimensional finite-volume model described in Tackley (1994) and used in Tackley (1993, 1996a,b) is employed. The  $8 \times 8 \times 1$  box is subdivided into  $128 \times 128$  uniformly spaced control volumes in the horizontal directions and 16 nonuniformly spaced control volumes in the vertical direction (vertical mesh spacing is such that the grid density is greater near the upper and lower boundaries). Test calculations in which the number of grid points is doubled in the vertical direction show no significant changes in the overall flow characteristics due to the higher resolution. This indicates that the number of grid points given above is adequate to resolve the flow features of interest to this study. Explicit timestepping of the energy equation is performed via a second order implementation of the MPDATA algorithm of Smolarkiewicz (1984). The continuity and momentum equations are solved via a multigrid algorithm developed along the lines of the method outlined by Brandt (1977, 1982).

Calculations are initialized with either the final

frame of a previously calculated convection solution or from a random initial state consisting of small amplitude ( $< \pm 10\%$ ) white noise added to a preselected vertical/radial temperature profile. For the spherical calculations, the conduction profile is used as the initial radial temperature profile. In cartesian geometry, an isothermal interior ( $T = 0.5$ ) is chosen as the initial temperature profile with error-function boundary layers at top and bottom. In both spherical and cartesian cases, calculations are allowed to evolve in time until the solutions pass sufficiently out of the phase of transient adjustment to initial conditions (judged by monitoring the temporal behavior of global quantities such as surface heat flow, r.m.s. velocity and mean temperature).

### 3. Fundamental transitions

The style of convection in a variable-viscosity fluid changes as the viscosity contrast across the fluid layer increases. At small viscosity contrasts, the cold fluid near the upper boundary is entirely mobile and participates freely in the convective motions. As viscosity contrasts grow larger ( $\Delta\mu \approx 100\text{--}1000$ ), cold fluid near the upper boundary becomes increasingly more viscous and is less able to participate in convective overturning; a sluggish lid of cold, viscous fluid develops. When the viscosity contrast is increased still further ( $\Delta\mu \approx 10^4$ ), the cold fluid at the upper surface becomes so viscous as to form a

stagnant lid, effectively ceasing to participate in the convective motions that occur below it.

The two fundamental transitions in the vertical structure of thermal convection (mobile lid to sluggish lid and sluggish lid to stagnant lid) have been identified numerically in small-domain, two-dimensional experiments (Christensen, 1984b; Moresi and Solomatov, 1995) on the basis of changes in the Nusselt number versus Rayleigh number relationship. In three-dimensional, small aspect ratio, cartesian geometry, the transitions were identified based on the vertical distribution of flow speeds (Ogawa et al., 1991). Solomatov (1995) has provided a theoretical overview of these transitions. Here, we present calculations which demonstrate that large a variation of viscosity (i.e., a strong temperature dependence of viscosity) induces dramatic changes in the horizontal planform of convection in addition to the above-mentioned changes in style of lid deformation.

Fig. 2 shows residual temperature isosurfaces, i.e., temperature relative to the horizontally-averaged geotherm, for both cartesian and spherical convection calculations with  $Ra_{1/2} = 10^5$  (the volume-averaged Rayleigh numbers for each of the variable viscosity calculations differ from  $Ra_{1/2}$  by less than a factor of  $\sim 3$ ). These images show the dramatic change in convective planform that occurs with increasing viscosity contrast. For isoviscous flow ( $\Delta\mu = 1$ ) in cartesian geometry, upwellings and downwellings both exhibit a sheet-like structure and the wavelength of the flow pattern is somewhat large

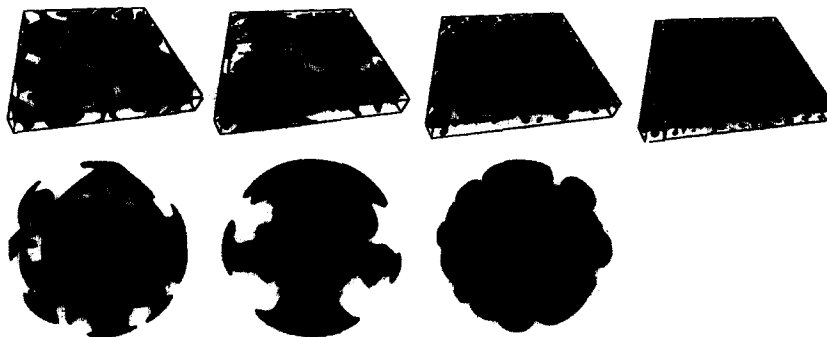


Fig. 2. The residual temperature isosurfaces for convection at  $Ra_{1/2} = 10^5$  in cartesian (top) and spherical (bottom) geometries. The viscosity contrasts, from left to right are  $\Delta\mu = 1, 10^3, 10^4, 10^5$ . The residual temperature levels are: Cartesian:  $\delta T = \pm 0.1, \pm 0.1, \pm 0.075, \pm 0.05$ ; Spherical:  $\delta T = (+0.2, -0.15), (+0.2, -0.15), \pm 0.15$ . Lighter surfaces indicate hot (upwelling) fluid. Darker surfaces indicate cold (downwelling) fluid. The lower boundary of the spherical shell is displayed with the lightest shading.

compared to the depth of the layer. In the spherical shell, the isoviscous flow is dominated by arcuate downwelling sheets and plume-like upflow; flow wavelength is of scale similar to the cartesian calculation. At  $\Delta\mu = 10^3$ , both spherical and cartesian calculations are in the sluggish-lid regime of convection. For both geometries, the wavelengths of flows have increased dramatically and the structures of the dominant upwelling and downwelling features have changed as well. Downwelling flow in the sluggish-lid regime occurs in the form of quasi-cylindrical structures. In the box, upwelling occurs as long, linear sheets, and for the spherical shell as a linear

chain of partially connected plumes in the equatorial region. The stagnant-lid regime is reached in both the cartesian box and the spherical shell when  $\Delta\mu = 10^4$ . Once again, a dramatic change in flow pattern occurs for both geometries. The wavelengths of the flow patterns decrease remarkably. In addition, the relative nature of upwelling and downwelling in the stagnant-lid regime has reversed compared to the sluggish-lid cases. Upwelling flow in both geometries is now dominated by numerous, small-scale cylindrical plumes; downwelling flow occurs as an inter-connected network of short, sheet-like features. The Cartesian calculation at  $\Delta\mu = 10^5$  shows that

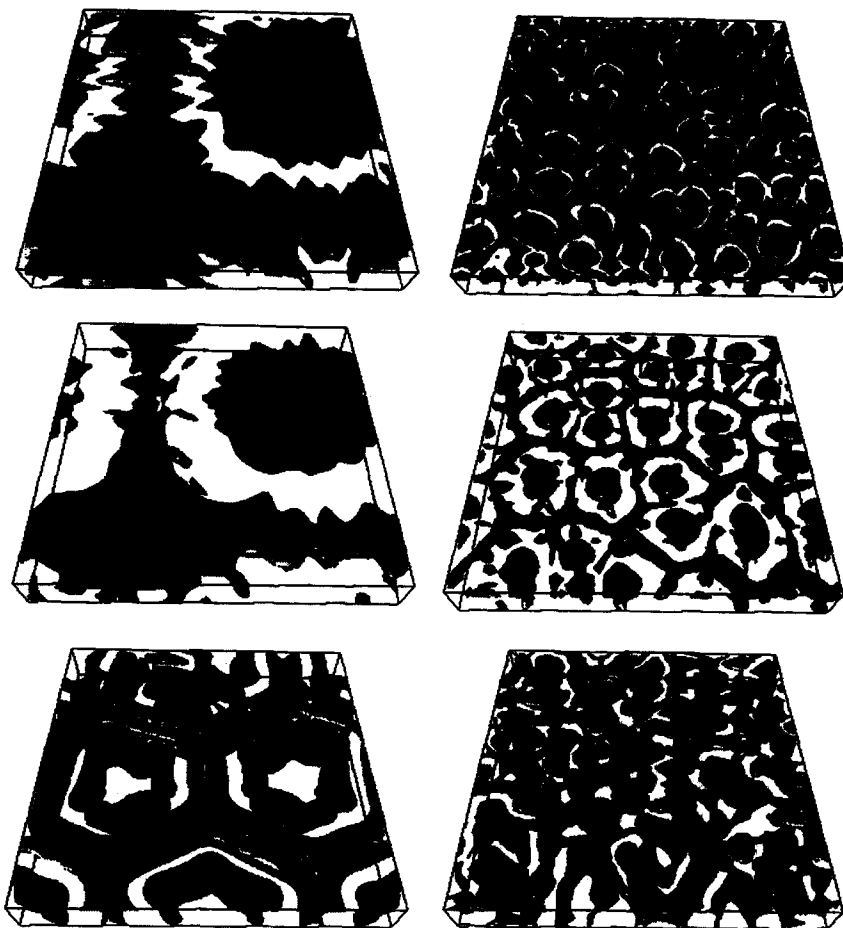


Fig. 3. The residual temperature isosurfaces for sluggish-lid (left) and stagnant-lid (right) convection at  $Ra_{1/2} = 10^5$  in cartesian geometry with different temperature-dependent viscosity structures. Top:  $\mu = \mu(T)$ , fully three-dimensional viscosity variations,  $\Delta\mu = 10^3$  and  $\Delta\mu = 10^5$ , respectively. Center:  $\mu = \langle \mu(T) \rangle$ , vertical viscosity variations. Bottom:  $\mu = \mu(T) / \langle \mu(T) \rangle$ , horizontal viscosity variations.  $\langle \cdot \rangle$  indicates a horizontal average. Lighter shading is hot upwelling flow, darker shades represent cold downwelling fluid.

no additional planform transition occurs in the viscosity contrast interval  $10^4$  to  $10^5$ .

The large changes in convective planform induced by strongly temperature-dependent viscosity raises an intriguing question. Which aspect of the viscosity variation is of greater importance: horizontal variations or vertical variations? The answer to this question is important since the most effective means of determining the viscosity structure of the mantle, namely geoid modelling and inversion of post-glacial rebound data, do not take into account lateral variations in viscosity (Peltier, 1989; King, 1995).

In order to address this question, additional cartesian calculations are undertaken using the sluggish-lid and stagnant-lid results, discussed above, as control models. To examine the effects of vertical viscosity variations, calculations similar to the control models are performed wherein the full three-dimensional viscosity is calculated from Eq. (3) at each timestep but is then averaged horizontally at each level before being used in the momentum equations. This treatment results in strictly vertical variations in viscosity. Predominantly horizontal viscosity variations are achieved by normalizing, at each timestep, the three-dimensional viscosity field by the horizontally-averaged viscosity at each vertical level; there is thus no vertical variation in the mean viscosity. Each case was initialized with a very short-wavelength flow pattern in order to insure that the final planform was not influenced by any bias in the initial conditions.

The results of this experiment are illustrated in Fig. 3 which shows residual temperature isosurfaces for sluggish-lid and stagnant-lid convective flows with a fully three-dimensional viscosity structure, vertical viscosity variations only, and predominantly horizontal viscosity variations. To first order, the convective patterns obtained with strictly vertical viscosity variations are the same as in the calculation with fully temperature-dependent viscosity. The patterns obtained using mostly horizontal viscosity variations are more similar to each other than to any of the cases with vertical viscosity structure. This suggests that the dominant factor influencing the scale of three-dimensional convection with temperature-dependent viscosity is the strength of the vertical variations that arises out of the temperature-dependence.

At first glance, it is tempting to draw parallels for the shift to long wavelengths (i.e., reddening of the spectra) in the sluggish-lid cases with vertical viscosity variations to the recent work of Bunge et al. (1996) in which reddening of the heterogeneity spectrum was also linked to vertical variations in viscosity. There is an important distinction to be made, however. Bunge et al. (1996) employ a factor of 30 increase in the viscosity of the lower mantle. In this respect, the results of Bunge et al. (1996) are more akin to the two-dimensional cartesian study by Davies (1988). In the cases considered here, the mantle outside of the thermal boundary layers is, on average, of uniform viscosity. Due to the temperature structure, the lower mantle of the current calculations can actually be less viscous than the upper mantle by an amount which depends on both the viscosity contrast and the temperature structure.

#### **4. Effect of boundary conditions**

Although the estimated viscosity contrast between the Earth's lithosphere and mantle would seem to indicate that the Earth should be in the stagnant-lid mode of convection, the surface expression of convection in the Earth (i.e., plate tectonics) indicates that this is not the case. Lithospheric plates on the Earth are in constant motion, being cyclically created and destroyed at plate margins (spreading centers and subduction zones, respectively). An important phenomenon, present in the actual lithosphere of the Earth but missing in the previously discussed convection models, is the presence of lithospheric faults. Faults act to break up the otherwise rigid lithosphere into separate plates, forming the relatively weak margins where subduction or spreading can be initiated. A simple test of the influence of faulting on stagnant-lid convection can be achieved by taking one of the stagnant-lid cases from Fig. 2 and specifying surface weak zones, i.e., selecting regions in the stiff upper boundary layer where viscosity is artificially reduced to mimic the effect of faulting. Such weak zones are commonly used to provide a first-order representation of lithospheric faults in mantle convection studies (Gurnis, 1989; Cserepes and Christensen, 1990; King et al., 1992; Zhong and Gurnis, 1994). Although such an ad hoc specification

of weak zones cannot address how faults originate or evolve, it can examine how the presence of faults affects the underlying mantle flow.

The cartesian, stagnant-lid calculation with  $\Delta\mu = 10^5$  shown in Fig. 2 is used to test the influence of weak zones. Taking the stagnant-lid solution as an initial condition, regions of artificially low viscosity

are placed near the surface along the left and right side-wall boundaries of the box. These weak zones extend to a depth equal to about 0.1 of the layer thickness wherein the dimensionless viscosity is forced to a value of unity. The side-wall boundary conditions are also made reflecting (as opposed to periodic) in order to permit longer wavelength flow

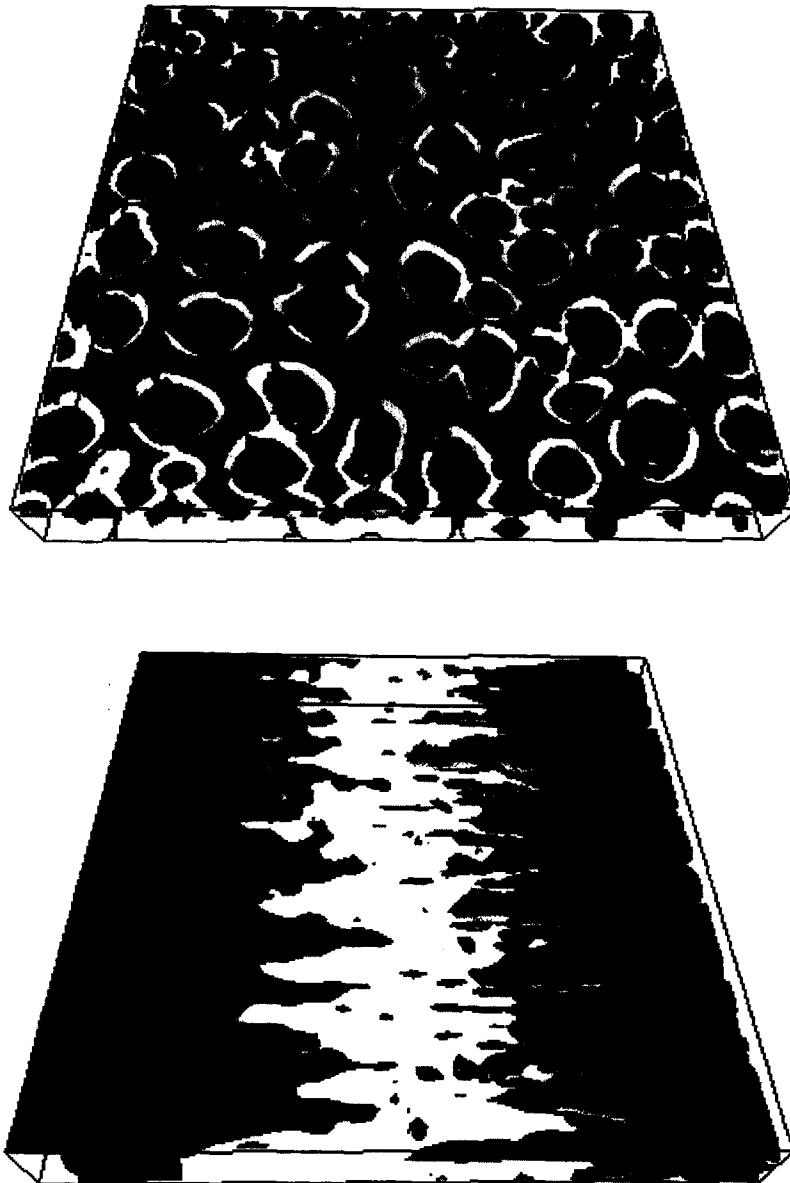


Fig. 4. The residual temperature isosurfaces for convection at  $Ra_{1/2} = 10^5$  in cartesian geometry with  $\Delta\mu = 10^5$ . Top: Stagnant-lid calculation, no weak zones (same as in Fig. 2). Bottom: Weak zones imposed along the left and right side boundaries.

to develop. Results of this calculation are displayed in Fig. 4. The inclusion of weak zones has a distinct effect on the style of convective flow. The stagnant-lid solution (no weak zones) is dominated by small-scale upwelling plumes embedded in a network of short, linear downwelling features. With the addition of weak zones, convection reorganizes into a single

large roll with small-scale Richter-type instabilities (Richter, 1973). Upwelling and downwelling flow occurs at the locations of the weak zones. The cold, stiff upper boundary layer behaves in the manner of an oceanic plate, spreading with a nearly uniform velocity from the right side of the box to the left. The much smaller Richter rolls are aligned such that

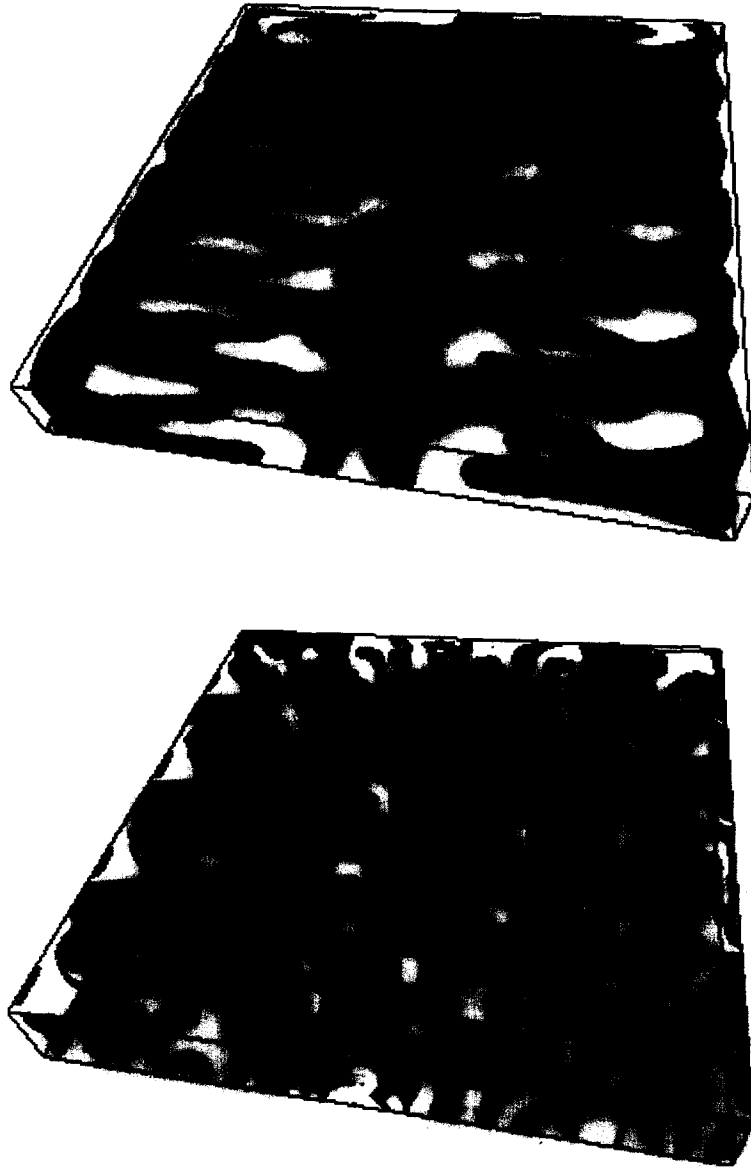


Fig. 5. The residual temperature isosurfaces for constant viscosity convection at  $Ra_{1/2} = 10^5$  with imposed plate-like surface velocities. Top: Two plates. Bottom: 64 plates. Lighter shading indicates hot, upwelling (divergent) flow, darker shading represents cold, downwelling (convergent) flow.

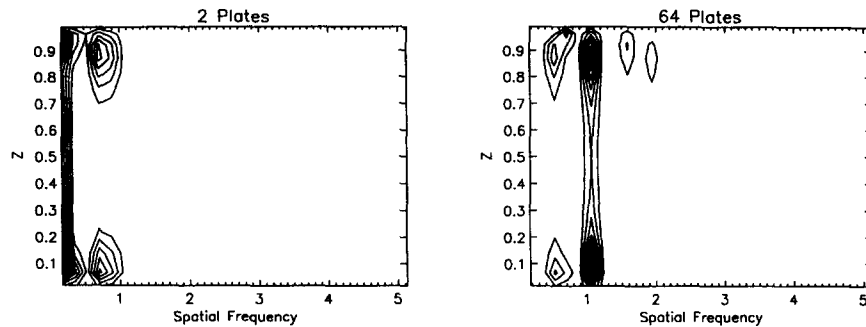


Fig. 6. The spectral heterogeneity maps showing spectral power as a function of depth for the convection calculations with imposed plate-like surface velocities. Heterogeneity maps for the 2-plate and 64-plate cases correspond to the flow patterns shown in Fig. 5.

the long axis of the rolls are parallel to the direction of the plate-like surface motion.

Another method that has been used to simulate plate-like behavior in convection calculations is to impose plate-like surface motion in the form of velocity boundary conditions (Davies, 1988; Bunge and Richards, 1996). To test the effect of plate-like surface velocities, two isoviscous calculations in cartesian geometry with imposed surface velocities (2 plates and 64 plates) are examined. In each of these calculations, the imposed surface velocity is chosen to match the r.m.s. surface velocity of the free-slip isoviscous calculation presented in Fig. 2. Fig. 5 illustrates the effect of imposing plate-like boundary velocities on convection calculations. In the two-plate calculation, the flow structure parallel to the imposed plate-like velocity adopts the wavelength of this surface forcing (convergent in the center of the box, divergent at the left and right side boundaries). Smaller scale Richter rolls (Richter, 1973) develop perpendicular to the imposed plate motion. With 64 surface plates, flow structure is again dominated by the form of the surface forcing. The locations of the upwelling and downwelling flow in this case are more closely dictated by the imposed zones of convergence and divergence (i.e., no Richter rolls). Examination of the spectral heterogeneity maps (Tackley et al., 1994) in Fig. 6, shows that in the two-plate case, the dominant heterogeneity is for the longest-wavelength mode. There is a secondary peak, at a spatial frequency of about 0.8, near the upper and lower boundaries which correspond to the scale of the Richter rolls. In the 64-plate case, the dominant spatial frequency at all depths is

about 1, corresponding to the imposed surface velocities. Thus in both cases, the boundary forcing controls the length-scale of the flow throughout the entire layer.

## 5. Conclusions

Strongly temperature-dependent viscosity can have dramatic effects on the style of convective flow as viscosity contrasts are increased. Two fundamental changes in horizontal planform occur which correspond to the transitions from mobile-lid to sluggish-lid flow and from sluggish-lid to stagnant-lid regimes of convection. These fundamental transitions occur in both cartesian geometry and in spherical-shell geometry; they can also occur when some or all of the heat driving convection is generated within the fluid (Ratcliff et al., 1996a). The horizontal scale of flow goes from moderate wavelengths in the mobile-lid regime to long wavelengths for a sluggish lid (i.e., reddening) to very short wavelengths in the presence of a stagnant lid. The morphologies of upwelling and downwelling flows are also affected by these transitions. Mobile-lid flow is characterized by sheet-like upwelling and downwelling in the cartesian box and by sheet-like downwelling and plume-like upwelling in the spherical shell. With a sluggish lid, sinking flow takes on the form of quasi-cylindrical downwelling plumes while upwelling occurs as rising sheets (linear chains of plumes in the spherical shell). Once viscosity contrasts are large enough for a stagnant lid to form, flow becomes characterized by small-scale upwelling

plumes embedded in a network of linear downwelling structures. The dominant factor influencing the overall horizontal scale of the convective patterns (at a given Rayleigh number) is the vertical variation of viscosity arising from its temperature dependence. This is in contrast to the change in length scale obtained by Bunge et al. (1996) using a viscosity increase at 660 km depth and indicates that more than one mechanism may be responsible for the long wavelength tomographic and geoid signatures in the Earth's mantle.

Since the Rayleigh number for these calculations is perhaps two orders of magnitude smaller than that characterizing convection in the mantles of Venus and the Earth, it is important to consider how these results should scale with Rayleigh number. Theory (Solomatov, 1995) and two-dimensional numerical results (Christensen, 1984b; Hansen and Yuen, 1993) indicate that the viscosity contrast associated with the transition to the stagnant-lid regime is independent of Rayleigh number, whereas the viscosity contrast associated with the transition from the mobile-lid to the sluggish-lid regime increases with increasing Rayleigh number. Thus, high Rayleigh number convection calculations with small viscosity contrasts (Balachandar et al., 1995a,b) are probably in the mobile-lid regime.

From a first-order comparison of Venus' surface with numerical results (Ratcliff et al., 1995), it appears that Venus may be in the sluggish-lid regime. Not only does the convective planform shown by Ratcliff et al. (1995) bear a striking similarity to the actual arrangement of surface features on Venus, but the observed tectonic deformation (Grimm, 1994) also suggests a sluggishly deforming, as opposed to a completely stagnant, lithosphere; this is a somewhat surprising result inasmuch as the expected viscosity contrast between the lithosphere and mantle of Venus should place the planet firmly in the stagnant-lid regime of convection. This could be due to the effects of non-Newtonian viscosity which act to reduce the total viscosity variation for a given activation energy (Christensen, 1983, 1984a) and/or to nonviscous deformation of the lithosphere that essentially reduces its 'effective' viscosity.

The regime of temperature-dependent viscosity convection that most closely resembles the surface expression of convection in the Earth is the mobile-lid

regime; however, this comparison is highly imperfect since complex material properties are required to describe the brittle failure that causes plate boundaries. Mimicking brittle faulting by imposing weak zones near the surface of convection calculations illustrates how important such nonviscous behavior can be in determining the character of convection in planetary mantles. Imposed weak zones change the style of convection from the small-scale flow of the purely stagnant-lid regime to a pattern completely governed by the arrangement of the weak zones. Inducing plate-like behavior through velocity boundary conditions also results in flow patterns completely governed by the prescribed surface forcing. In light of this, studies which induce plate-like behavior in this fashion must be interpreted with care. Such studies suggest that long-wavelength heterogeneity in the mantle is indeed affected by plate dimensions but tell us little about what physical mechanism dictates the size of tectonic plates or how feedback from mantle flow may affect plate sizes. Clearly, the existence of surface plates has a strong effect on the style of convection in the Earth and the formulation of methods to self-consistently generate plates in convection models remains an active and eagerly anticipated area of research (Weinstein and Olson, 1992; Bercovici, 1993; Bercovici and Wessel, 1994; Zhong and Gurnis, 1995).

## Acknowledgements

This research was supported by the NASA Geodynamics Program, grant NAGW 2646, and the National Science Foundation, grant EAR 9506683. Computational resources on the Cray C90 and Intel Paragon were provided by the San Diego Supercomputer Center. We thank David Yuen and an anonymous reviewer for helpful comments.

## References

- Balachandar, S., Yuen, D.A., Reuteler, D.M., 1995a. Localization of toroidal motion and shear heating in 3-D high Rayleigh number convection with temperature-dependent viscosity. *Geophys. Res. Lett.* 22, 477–480.
- Balachandar, S., Yuen, D.A., Reuteler, D.M., Lauer, G.S., 1995b.

- Viscous dissipation in 3-dimensional convection with temperature-dependent viscosity. *Science* 267, 1150–1153.
- Bercovici, D., 1993. A simple model of plate generation from mantle flow. *Geophys. J. Int.* 114, 635–650.
- Bercovici, D., Wessel, P., 1994. A continuous kinematic model of plate-tectonic motions. *Geophys. J. Int.* 119, 595–610.
- Booker, J.R., 1976. Thermal convection with strongly temperature-dependent viscosity. *J. Fluid Mech.* 76, 741–754.
- Brandt, A., 1977. Multi-level adaptive solutions for boundary-value problems. *Math. Comput.* 31, 333–390.
- Brandt, A., 1982. Guide to multigrid development. In: Hackbush, W., Trottenberg, U. (Eds.), *Lecture Notes in Mathematics*. Springer Verlag, Berlin, pp. 220–312.
- Bunge, H.P., Richards, M.A., 1996. The origin of large scale structure in mantle convection: Effects of plate motions and viscosity stratification. *Geophys. Res. Lett.* 23 (21), 2987–2990.
- Bunge, H.P., Richards, M.A., Baumgardner, J.R., 1996. The effect of depth-dependent viscosity on the plan-form of mantle convection. *Nature* 379 (6564), 436–438.
- Busse, F.H., 1989. Fundamentals of thermal convection. In: Peltier, W.R. (Ed.), *Mantle Convection: Plate Tectonics and Global Dynamics*. Gordon and Breach, New York, pp. 23–95.
- Christensen, U., 1983. Convection in a variable viscosity fluid: Newtonian versus non-Newtonian rheology. *Earth Planet. Sci. Lett.* 64, 153–162.
- Christensen, U., 1984a. Convection with pressure-dependent and temperature-dependent non-Newtonian rheology. *Geophys. J. Royal Astron. Soc.* 77, 343–384.
- Christensen, U., 1984b. Heat transport by variable viscosity convection and implications for the Earth's thermal evolution. *Phys. Earth Planet. Inter.* 206, 264–282.
- Christensen, U., Harder, H., 1991. 3-d convection with variable viscosity. *Geophys. J. Int.* 104, 213–226.
- Cserepes, L., Christensen, U., 1990. Three-dimensional convection under drifting plates. *Geophys. Res. Lett.* 17, 1497–1500.
- Davies, G.F., 1988. Role of the lithosphere in mantle convection. *J. Geophys. Res.* 93, 10451–10466.
- Giannandrea, E., Christensen, U.R., 1993. Variable viscosity convection experiments with stress-free upper boundary and implications for the heat-transport in the Earth's mantle. *Phys. Earth Planet. Inter.* 78, 139–152.
- Grimm, R.E., 1994. Recent deformation rates on Venus. *J. Geophys. Res.* 99 (E11), 23163–23171.
- Gurnis, M., 1989. A reassessment of the heat transport by variable viscosity convection with plates and lids. *Geophys. Res. Lett.* 16, 179–182.
- Hansen, U., Yuen, D.A., 1993. High Rayleigh number regime of temperature-dependent viscosity convection and the Earth's early thermal history. *Geophys. Res. Lett.* 20, 2191–2194.
- Hsui, A.T., 1978. A numerical simulation of finite-amplitude thermal convection with large viscosity variation in axisymmetric spherical geometry: Effect of mechanical boundary conditions. *Tectonophysics* 50, 147–162.
- King, S.D., 1995. The viscosity structure of the mantle. *Rev. Geophys.* 33, 11–17.
- King, S.D., Gable, C.W., Weinstein, S.A., 1992. Models of convection-driven tectonic plates: A comparison. *Geophys. J. Int.* 109, 481–487.
- Machetel, P., Rabinowicz, M., 1985. Transition to a two mode axisymmetrical spherical convection: Applications to the Earth's mantle. *Geophys. Res. Lett.* 12, 227–230.
- Moresi, L.N., Solomatov, V.S., 1995. Numerical investigation of 2D convection with extremely large viscosity variations. *Phys. Fluids* 7, 2154–2162.
- Ogawa, M., Schubert, G., Zebib, A., 1991. Numerical simulations of three-dimensional thermal convection in a fluid with strongly temperature-dependent viscosity. *J. Fluid Mech.* 233, 299–328.
- Patankar, S.V., 1980. *Numerical Heat Transfer and Fluid Flow*. Hemisphere, Washington, D.C.
- Peltier, W.R., 1989. Mantle viscosity. In: Peltier, W.R. (Ed.), *Mantle Convection: Plate Tectonics and Global Dynamics*. Gordon and Breach, New York, pp. 389–478.
- Ratcliff, J.T., Schubert, G., Zebib, A., 1995. Three-dimensional variable viscosity convection of an infinite Prandtl number Boussinesq fluid in a spherical shell. *Geophys. Res. Lett.* 22 (16), 2227–2230.
- Ratcliff, J.T., Schubert, G., Zebib, A., 1996a. Effects of temperature-dependent viscosity on thermal convection in a spherical shell. *Physica D* 97, 242–252.
- Ratcliff, J.T., Schubert, G., Zebib, A., 1996b. Steady tetrahedral and cubic patterns of spherical-shell convection with temperature-dependent viscosity. *J. Geophys. Res.* 101 (B11), 25473–25484.
- Richter, F.M., 1973. Convection and large-scale circulation of the mantle. *J. Geophys. Res.* 78, 8735–8745.
- Richter, F.M., 1978. Experiments on the stability of convection rolls in fluids whose viscosity depends on temperature. *J. Fluid Mech.* 89, 553–560.
- Richter, F.M., Nataf, H.C., Daly, S.F., 1983. Heat-transfer and horizontally averaged temperature of convection with large viscosity variations. *J. Fluid Mech.* 129, 173–192.
- Schubert, G., 1979. Subsolidus convection in the mantles of terrestrial planets. *Annu. Rev. Earth Planet. Sci.* 7, 289–342.
- Smolarkiewicz, P.K., 1984. A fully multidimensional positive definite advection transport algorithm with small implicit diffusion. *J. Comput. Phys.* 54, 325–362.
- Solomatov, S.V., 1995. Scaling of temperature- and stress-dependent viscosity convection. *Phys. Fluids* 7, 266–274.
- Stengel, K.C., Oliver, D.S., Booker, J.R., 1982. Onset of convection in a variable-viscosity fluid. *J. Fluid Mech.* 120, 411–431.
- Tackley, P.J., 1993. Effects of strongly temperature-dependent viscosity on time-dependent, three-dimensional models of mantle convection. *Geophys. Res. Lett.* 20, 2187–2190.
- Tackley, P.J., 1994. Three-dimensional models of mantle convection: Influence of phase transitions and temperature-dependent viscosity. Ph.D. Thesis, California Institute of Technology.
- Tackley, P.J., 1996a. Effects of strongly variable viscosity on three-dimensional compressible convection in planetary mantles. *J. Geophys. Res.* 101, 3311–3332.
- Tackley, P.J., 1996b. On the ability of phase transitions and viscosity layering to induce long-wavelength heterogeneity in the mantle. *Geophys. Res. Lett.* 23, 1985–1988.
- Tackley, P.J., Stevenson, D., Glatzmaier, G.A., Schubert, G.,

1994. Effects of multiple phase transitions in a 3D spherical model of convection in the Earth's mantle. *J. Geophys. Res.* 99, 15877–15901.
- Weertman, J., 1970. The creep strength of the Earth's mantle. *Rev. Geophys.* 8, 145–168.
- Weertman, J., Weertman, J.R., 1975. High temperature creep of rock and mantle viscosity. *Annu. Rev. Earth Planet. Sci.* 3, 293–315.
- Weinstein, S., Christensen, U., 1991. Convection plan-forms in a fluid with a temperature-dependent viscosity beneath a stress-free upper boundary. *Geophys. Res. Lett.* 18, 2035–2038.
- Weinstein, S., Olson, P., 1992. Thermal convection with non-Newtonian plates. *Geophys. J. Int.* 111, 515–530.
- White, D.B., 1988. The plan-forms and onset of convection with temperature-dependent viscosity. *J. Fluid Mech.* 191, 247–286.
- Zebib, A., 1993. Linear and weakly nonlinear variable viscosity convection in spherical shells. *Theor. Comput. Fluid Dyn.* 4, 241–253.
- Zhong, S., Gurnis, M., 1994. Role of plates and temperature-dependent viscosity in phase-change dynamics. *J. Geophys. Res.* 99, 15903–15917.
- Zhong, S., Gurnis, M., 1995. Towards a realistic simulation of plate margins in mantle convection. *Geophys. Res. Lett.* 22, 981–984.